

Energy Transfer in the Peridinin Chlorophyll-*a* Protein of *Amphidinium carterae* Studied by Polarized Transient Absorption and Target Analysis

Brent P. Krueger,* Stefania S. Lampoura,* Ivo H. M. van Stokkum,* Emmanouil Papagiannakis,* Jante M. Salverda,* Claudiu C. Gradinaru,* Danielis Rutkauskas,* Roger G. Hiller,[†] and Rienk van Grondelle*

*Department of Physics and Astronomy, Vrije Universiteit, 1081 HV Amsterdam, The Netherlands; and [†]School of Biological Sciences, Macquarie University, NSW 2109, Australia

ABSTRACT The peridinin chlorophyll-*a* protein (PCP) of dinoflagellates differs from the well-studied light-harvesting complexes of purple bacteria and green plants in its large (4:1) carotenoid to chlorophyll ratio and the unusual properties of its primary pigment, the carotenoid peridinin. We utilized ultrafast polarized transient absorption spectroscopy to examine the flow of energy in PCP after initial excitation into the strongly allowed peridinin S_2 state. Global and target analysis of the isotropic and anisotropic decays reveals that significant excitation (25–50%) is transferred to chlorophyll-*a* directly from the peridinin S_2 state. Because of overlapping positive and negative features, this pathway was unseen in earlier single-wavelength experiments. In addition, the anisotropy remains constant and high in the peridinin population, indicating that energy transfer from peridinin to peridinin represents a minor or negligible pathway. The carotenoids are also coupled directly to chlorophyll-*a* via a low-lying singlet state S_1 or the recently identified S_{CT} . We model this energy transfer time scale as 2.3 ± 0.2 ps, driven by a coupling of ~ 47 cm⁻¹. This coupling strength allows us to estimate that the peridinin S_1/S_{CT} donor state transition moment is ~ 3 D.

INTRODUCTION

Carotenoids are perhaps the most ubiquitous pigments in nature, serving as antioxidants in organisms ranging in complexity from single-celled to higher mammals (Britton and Young, 1993; van Grondelle et al., 1994; Frank and Cogdell, 1996; Koyama et al., 1996). In photosynthetic organisms carotenoids serve a second role as light-harvesting pigments. The latter role has received considerable attention recently as the complex photophysics of carotenoids has become better understood (Hudson et al., 1982; Andersson et al., 1991, 1995; DeCoster et al., 1992; Frank et al., 1993; Chynwat and Frank, 1995; Fujii et al., 1998; Herek et al., 1998; Sashima et al., 1998; Krueger et al., 1999a,b; Polivka et al., 1999; Sundström et al., 1999), and the crystal structures of several light-harvesting complexes have become known (Kühlbrandt et al., 1994; McDermott et al., 1995; Hofmann et al., 1996; Koepke et al., 1996; Schubert et al., 1997). In this work, we report the results of ultrafast transient absorption studies that examined electronic excitation transfer (EET) between carotenoids and chlorophylls in the peridinin chlorophyll-*a* protein (PCP) light-harvesting complex from the dinoflagellate *Amphidinium carterae*. These experiments reveal that significant excitation is transferred directly from the peridinin S_2 state to chlorophyll-*a* (Chl*a*) in competition with rapid internal

conversion from peridinin S_2 to an equilibrium between S_1 and a third low-lying singlet state, S_{CT} , identified recently (Bautista et al., 1999a; Sashima et al., 1999; Frank et al., 2000). Fast peridinin to Chl*a* energy transfer is also mediated by coupling of the peridinin S_1 or S_{CT} transition to the Chl*a*. The magnitude of this coupling suggests a peridinin S_1/S_{CT} transition dipole moment of ~ 3 D. The experiments do not show evidence of significant peridinin-peridinin energy transfer. (Note that we adopt the typical notation in which the S_2 and S_1 states of peridinin correspond to the $1B_u^+$ and $2A_g^-$ states of ideal C_{2h} symmetry, respectively. By analogy, the S_{CT} state would correspond to $1B_u^-$, although this relationship is not known and is complicated by the asymmetry of peridinin.)

Light-harvesting complexes (LHCs) play a vital role in photosynthetic organisms (Clayton, 1980; Sundström et al., 1999; Govindjee, 2000) by absorbing sunlight and efficiently transferring the resulting electronic excitation energy to the reaction center where the energy is converted to a charge separation that drives the further, chemical processes of photosynthesis. To carry out their role, most light-harvesting pigments (e.g., chlorophylls) display strong absorption throughout the visible spectrum, maximizing absorption of sunlight, along with high fluorescence quantum yields made possible via large radiative rates and long singlet lifetimes, maximizing energy donor functionality. The ability of carotenoids to serve as light-harvesting pigments is a bit enigmatic because, while showing a strong, broad absorption into their S_2 state, their fluorescent quantum yields are tiny (Frank and Cogdell, 1996; Koyama et al., 1996). The lack of fluorescence is due to rapid internal conversion from the S_2 to the optically forbidden S_1 state (see Fig. 1). Thus, although the S_2 state has a strong transition dipole (to/from S_0) it is difficult for energy transfer to

Received for publication 25 April 2000 and in final form 19 March 2001.

Address reprint requests to Dr. Rienk van Grondelle, Vrije Universiteit, Department of Physics and Astronomy, DeBoelelaan 1081 HV, Amsterdam, Netherlands. Tel: 31204447930; Fax: 31204447999; E-mail: rienk@nat.vu.nl.

Dr. Krueger's present address is Hope College, Chemistry Dept., Peale Science Center, 35 E. 12th St., Holland, MI 49422-9000.

© 2001 by the Biophysical Society

0006-3495/01/06/2843/13 \$2.00

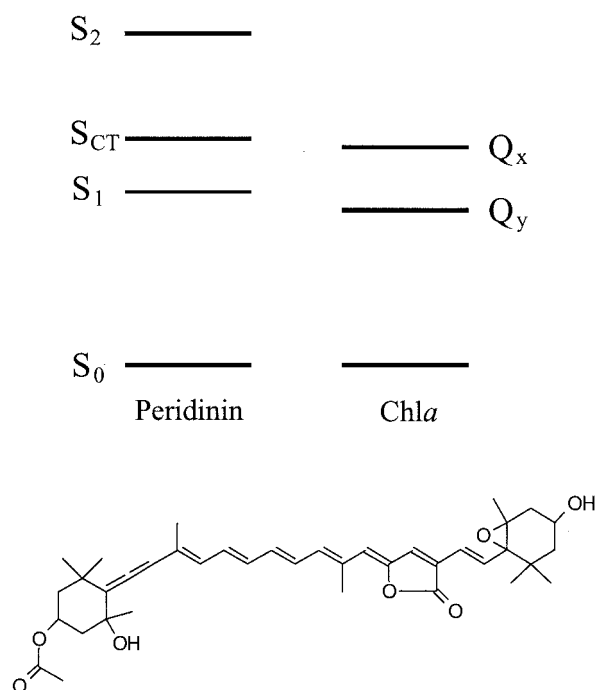


FIGURE 1 A schematic diagram of the states relevant to EET in PCP. The peridinin S_1 , S_{CT} , and S_2 states are given along with the Chla Q_x and Q_y states. The relative energies of the states are approximate, particularly for S_1 and S_{CT} . Below is the chemical structure of peridinin.

compete with the rapid internal conversion (i.e., short S_2 lifetime). In contrast, the S_1 state has a forbidden transition dipole (to/from S_0), which disallows traditional long-range coupling mechanisms such as Förster theory (Förster, 1948, 1965), making EET difficult despite a reasonable S_1 lifetime (10–100 ps). Nature has succeeded in utilizing carotenoids as light-harvesting pigments by placing them very close to a group of energy-accepting pigments, typically chlorophylls. Thus, the carotenoid S_2 transition can couple strongly to several chlorophylls, resulting in rapid EET that can, in some cases, compete with the S_2 - S_1 internal conversion (Shreve et al., 1991; Andersson et al., 1996; Peterman et al., 1997a; Krueger et al., 1998); and the dipole-forbidden carotenoid S_1 transition can have significant coupling through higher-order transition multipoles and orbital overlap mechanisms, which are too weak at longer distances (Nagae et al., 1993; Scholes et al., 1997; Damjanovic et al., 1999).

Here, we examine the PCP light-harvesting complex from the dinoflagellate *Amphidinium carterae*. Previous studies have shown that PCP differs from other carotenoid-based light-harvesting complexes both in EET pathways and in its primary pigment, peridinin. Although the light-harvesting complexes from purple bacteria all exhibit significant carotenoid S_2 →bacteriochlorophyll EET (Shreve et al., 1991; Andersson et al., 1996; Ricci et al., 1996; Krueger et al., 1998), experiments on PCP have suggested that all

peridinin→Chla EET is mediated by the S_1 state (Akimoto et al., 1996; Bautista et al., 1999b). Presumably, this is due to the unusual photophysical properties of peridinin. Typical carotenoids, such as β -carotene, consist of a C_{2h} symmetric polyene backbone that is mainly unsubstituted. Peridinin, whose structure is given in Fig. 1 along with the relevant energy levels of peridinin and Chla, has both a lactone ring and an allene moiety. These substituents break its C_{2h} symmetry, modifying the electronic structure of peridinin, yielding a carotenoid with significant emission (Mimuro et al., 1992; Akimoto et al., 1996) from, presumably, the S_1 state. Typical photosynthetic carotenoids from higher plants or bacteria show no S_1 emission and only small amounts of S_2 emission (DeCoster et al., 1992); however, the oxygenated carotenoids (e.g., peridinin, fucoxanthin, and siphonaxanthin) characteristic of several algal groups exhibit a weak S_1 emission (Mimuro et al., 1992). Experimental work (Bautista et al., 1999a; Frank et al., 2000) along with recent calculations (Damjanović et al., 2000) have suggested that the reduced symmetry of peridinin (compared with that of most carotenoids), particularly the presence of the carbonyl group in conjugation with the polyene backbone, relaxes the forbiddenness of the S_1 ↔ S_0 transition enough to allow emission, although S_1 absorption has not been observed. In addition, Frank and coworkers suggested that an additional electronic state with significant charge transfer character, S_{CT} , lies between the S_1 and S_2 states, complicating the situation (see Fig. 1). This state may be related to the $1B_u^-$ state recently observed in several carotenoids (Sashima et al., 1999, 2000), although the asymmetry of peridinin makes use of the C_{2h} symmetry labels more tenuous than for other carotenoids. Thus, the pathways and mechanisms of energy transfer from carotenoid to chlorophyll may be quite different in PCP relative to other light-harvesting complexes, and their identification is the primary motivation of the present investigation.

The crystal structure of PCP (Hofmann et al., 1996) reveals close contacts between groups of pigments. The smallest pigment unit consists of four peridinin surrounding a central chlorophyll-*a* (Chla). Two such groups of 4 peridinin and 1 Chla lie beside each other in each protein subunit, and subunits are further grouped as trimers containing 6 Chla and 24 peridinin. The close interactions between peridinin and the large ratio of peridinin to Chla suggest that peridinin-peridinin coupling could be strong and that energy may be transferred from peridinin to peridinin before peridinin-Chla transfer.

In this work, we present the results of ultrafast, polarized transient absorption spectroscopy on PCP. First, we describe the experiment along with our modeling procedures, followed by a brief description of the results in terms of a simple model. The Discussion presents a more detailed analysis using two more complex models, in which we show evidence for previously unseen peridinin S_2 →Chla EET on a ~100-fs time scale. We find no evidence of peridinin-

peridinin EET and model the peridinin S_1/S_{CT} -Chla EET time to be 2.3 ± 0.2 ps. Finally, this energy transfer rate is used to estimate the peridinin S_1/S_{CT} -Chla coupling strength, which in turn leads to an estimate of the transition dipole magnitude of the peridinin S_1/S_{CT} state of ~ 3 D.

MATERIALS AND METHODS

PCP samples were prepared as done previously (Sharples et al., 1996). Transient absorption experiments were carried out with ~ 4 ml of sample, which was flowed using a peristaltic pump and cooled in an ice-water bath. Steady-state absorption spectra were taken with a spectrophotometer (Perkin-Elmer $\lambda 40$) and emission spectra with a home-built fluorometer (Ar laser excitation, Oriel 77250 monochromator).

Transient absorption spectra were collected with a high-throughput diode array spectrometer that is described elsewhere (Gradinaru et al., 2000). Briefly, signal and reference probe spectra along with the pump intensity were measured for each of $\sim 10,000$ laser shots per time delay. Statistics of the pump intensity allowed each spectrum to be classified as pump on, pump off, or neither (pump intensity not within 10% of average), which were discarded. In addition, shots with probe spectra that were significantly different than the average probe spectra (from a single time delay) were also discarded. The average of the remaining signal and reference spectra with both pump on and pump off were combined in the standard fashion to yield a $\Delta O.D.$ spectrum. Spectral resolution of the system is ~ 0.5 nm and the spectral range is ~ 125 nm. Two separate sets of data were combined to yield the final probe window of ~ 450 – 700 nm.

Samples were excited by ~ 20 -nJ pulses of 500- or 520-nm light focused to a ~ 150 - μm -diameter spot, resulting in excitation densities of $\sim 10^{14}$ photons pulse $^{-1}$ cm $^{-2}$. Fitting $S = aP^x$ where S is transient absorption signal and P is pump power (varied from 20 to 180 nJ/pulse) gave $x \approx 0.9$, indicating the presence of mild annihilation and/or saturation. To guard against this, we have carefully performed measurements with both ~ 20 and ~ 100 nJ/pulse pump energy and found EET time scales that agree, confirming that any annihilation effects are within our reported experimental uncertainties.

Tunable excitation light was provided by a home-built, single-pass optical parametric amplifier. The OPA was pumped by a portion of the output from a Nd:YLF (B.M. Industries, Totowa, NJ, Q-switched maximum of 3 kHz) -pumped Ti:sapphire regenerative amplifier (B.M. Industries) that produced 500- μJ , 50-fs pulses at 1 kHz. The amplifier was seeded by 25-fs pulses from a Ti:sapphire oscillator (Coherent Mira, Santa Clara, CA) pumped by a diode-pumped Nd:YAG source (Coherent Verdi). The remaining output of the amplifier passed a delay line and was focused into a 2-mm sapphire window to produce multi-filament white light used as the probe. The probe beam was split into signal and reference and passed through a thin film polarizer before focusing on the sample. The signal and reference beams were collimated and dispersed off a single grating onto separate photodiode arrays for detection. The chopped pump beam passed a Berek polarization compensator (New Focus 5540, San Jose, CA), allowing it to be easily adjusted to parallel, perpendicular, and magic angle polarizations with minimal displacement of the beam. For all spectra, parallel and perpendicular data were used to construct magic angle curves for comparison with the actual magic angle data. No significant differences were found.

The instrument response function (IRF), fit to a Gaussian in the data sets, was 100–150 fs full-width half-maximum, similar to values obtained by measuring the rise of induced birefringence in CS $_2$. The probe pulse dispersion was fit as a third-order polynomial function of the wavelength. Imprecision in the IRF leads to errors in the fastest component in the fitting (e.g., species A of model I; cf. Fig. 3), which are reflected in the reported error bars. These errors are particularly problematic for the bluest wavelengths (< 530 nm) and in regions where artifacts such as scattered pump light or transient hole burning may influence the most rapid decay rate. To

reduce the effect of these artifacts on the measured rates, the 450–550-nm region was weighted lightly in the fitting process. Consequently, the shapes of the species-associated difference spectra (SADS) in this region are unreliable, particularly for the fastest component.

The data were analyzed using a global fitting routine (van Stokkum et al., 1994) as described previously. SADS were determined through target analysis assuming one of several models described later (cf. Fig. 3). The anisotropic data were fit by creating model isotropic (ma) and anisotropic (r) decay curves for each species (k). Parallel and perpendicular fits were then constructed via

$$\begin{bmatrix} MA_k(t) \\ VV_k(t) \\ VH_k(t) \end{bmatrix} = \begin{bmatrix} ma_k(t) \\ ma_k(t) \times (1 + 2r_k(t)) \\ ma_k(t) \times (1 - r_k(t)) \end{bmatrix} \otimes IRF(t), \quad (1)$$

in which \otimes means convolution, and combined to yield curves representing the full sample. The total error of the magic angle (MA), parallel (VV), and perpendicular (VH) fits compared with the respective data sets was used as the basis for improving the model isotropic and anisotropic decays. This associative fitting of the anisotropy (Brand et al., 1985) avoids difficulties that can arise from the discontinuities often observed in absorption anisotropy when spectrally overlapping species simultaneously contribute positive and negative signals (Jonas et al., 1996).

Two types of anisotropy models were employed. In the simpler model, the anisotropy of each species was assumed to have a constant value. In the more complicated scheme, the anisotropy of each species was allowed to decay, simulating intra-species (e.g., peridinin S_1 -peridinin S_1) EET. For both methods the total initial anisotropy, $r(0)$, was originally allowed to vary and always resulted in values near 0.40. Therefore, final fits were performed with the initial anisotropy fixed to $r(0) = 0.40$.

RESULTS

Steady-state absorption and emission spectra of PCP are shown in the upper panel of Fig. 2, with solution spectra of peridinin and Chla in the lower panel. Peridinin (S_2 transition) contributes the broad absorption from 400–550 nm whereas Chla contributes the peaks at 430 nm and 670 nm along with vibronic features just to the blue of these bands.

Because of the complexity of the multi-wavelength, difference-spectra data, perhaps the clearest presentation is in terms of a fit to a simple model. We expect the data to separate into three time scales, corresponding roughly with population of the peridinin S_2 state, the peridinin S_1 and S_{CT} states, and Chla. Therefore, a minimal model must contain three species, such as model I shown in Fig. 3, in which each model species corresponds to an average of the actual sample species that decay on a given time scale. The SADS that result from fitting model I to the isotropic data are shown in Fig. 4 and described briefly below. In addition, decay profiles of both the fit and the raw data (from isotropic 500-nm excitation) at several individual wavelengths, including 521 nm (primarily peridinin S_2 bleach), 570 nm (primarily peridinin S_1 excited state absorption), and 671 nm (primarily Chla Q_y bleach), are given in Fig. 5. Note that although there are some differences between the 500- and 520-nm excitation data, particularly in the noisy blue region (425–550 nm), the spectral features are similar and the lifetimes derived from fitting are the same. Thus, results

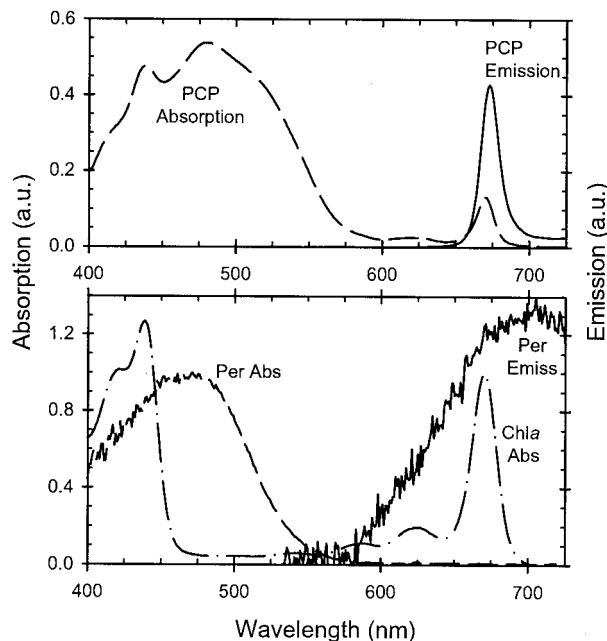


FIGURE 2 (Top) Absorption (— — —) and emission (—) spectra of PCP; (Bottom) Solution (methanol) spectra of the individual pigments in PCP. The peridinin absorption and emission spectra are given by dashed and solid lines, respectively, whereas the Chla absorption spectrum is given by the dashed-dotted line.

reported below are averages over both excitation wavelengths unless specifically noted.

The A species (primarily peridinin S_2) shows strong bleaching (negative signal) in the region of $S_2 \leftarrow S_0$ absorption as expected, along with excited-state absorption (ESA; positive signal) at longer wavelengths, which is more suggestive of peridinin S_1 or S_{CT} population, and a slight Chla bleach feature at 670 nm. The B species (primarily peridinin S_1 and S_{CT}) shows the anticipated strong excited-state absorption in the $S_n \leftarrow S_1$ region, from 550 to 620 nm, which continues farther red beyond 700 nm due to $S_n' \leftarrow S_{CT}$ absorption (see below), as well as the continued Chla bleach at 670 nm. The C species (primarily Chla) displays strong Q_y bleaching near 670 nm along with small amounts of ESA at bluer wavelengths, which appears to be a long-lived peridinin S_1 or perhaps T_1 population. Average characteristic time scales from the fitting of all data sets are <0.2 ps for the $A \rightarrow B$ step, 2.0 ± 0.2 ps for the $B \rightarrow C$ step and >1 ns for the decay of C.

Although model I does fit the data quite well, indicating that dynamics in PCP can be separated into three time scales (<200 fs, ~ 2 ps, and >1 ns), the resulting SADS demonstrate that model species A, B, and C all correspond to multiple PCP species. Species A contains characteristics of peridinin S_2 , S_{CT} , and S_1 as well as Chla. Species B contains peridinin S_1 and S_{CT} with Chla. Even species C, which is primarily Chla, contains evidence of some long-lived excited peridinin species.

Therefore, we developed models II and III (Fig. 3) to give a closer correspondence between model species and pathways with actual PCP species and pathways. The presence of strong S_1/S_{CT} characteristics in both species A and B suggests that two S_1 -like species are needed to encompass the two time scales of dynamics, which we label S_1 and S_{CT} . (The S_{CT} state may correspond to vibrationally excited S_1 rather than a separate electronic state. See Discussion.) The presence of Chla bleach in all species may be the result of rapid peridinin S_2 -Chla EET (model II) or direct excitation of Chla (model III). Finally, the presence of peridinin character in species C suggests a population of long-lived peridinin that does not transfer energy to Chla and is represented by the disconnected S_{1N} . Transfer to S_{1N} (through k_N) does not necessarily represent a physical process, but simply the fraction of population, $k_N/(k_N + k_3 + k_5)$, in the disconnected peridinin. The SADS that result from fitting models II and III to the 500-nm excitation data are given in Fig. 6 (expanding the red region to show more detail), and the rates of the pathways are given in Table 1.

Detailed description of the SADS and rates are left to various sections of the Discussion, although we provide several observations here. Each of the SADS correspond much closer to a single PCP species than the model I SADS, with the exception of S_{1N} , which, because of possible picosecond Chla relaxation (see below) and the small population of S_{1N} , still shows significant contamination from Chla. For both models II and III, the S_2 SADS are free from ESA and the Chla SADS are free of peridinin character, and for model II the S_2 , S_{CT} , and S_1 SADS are free of Chla bleach. Models II and III also differ in the amplitudes of S_{CT} and S_1 ESA relative to the Chla bleach. The amount of S_{1N} population (the value of k_N) is inferred from its contribution to the fit assuming a SADS amplitude similar to that of S_1 . The S_{1N} population is 10% of the S_1 population for the 520-nm excitation data and 20% for the 500-nm excitation data, suggesting that the non-EET peridinin population is generally blue-shifted of the EET peridinin population.

Fitting the anisotropy data to model II in the simplest way, in which all species have a constant anisotropy value, yields $R_{S_2} = 0.40$, $r_{S_{1N}} = r_{S_{CT}} = r_{S_1} = 0.29 \pm 0.05$, and $r_{Chla} = 0.06 \pm 0.05$. As mentioned in Materials and Methods, r_{S_2} was initially fit freely and always yielded values near 0.40, so this value was fixed in the final fits. Fig. 7 shows the experimental and model traces for all polarizations at several wavelengths. The wavelengths shown are particularly challenging to fit because they each reflect different and changing proportions of S_1/S_{CT} and Chla signals. Careful fitting allowing the anisotropy of each species to be time dependent yields no improvement to the fits. Therefore, only the results of the minimal model are reported. In an extended target analysis we could also identify contributions to the anisotropy decay from Chla-Chla energy transfer (Kleima et al., 2000a) on

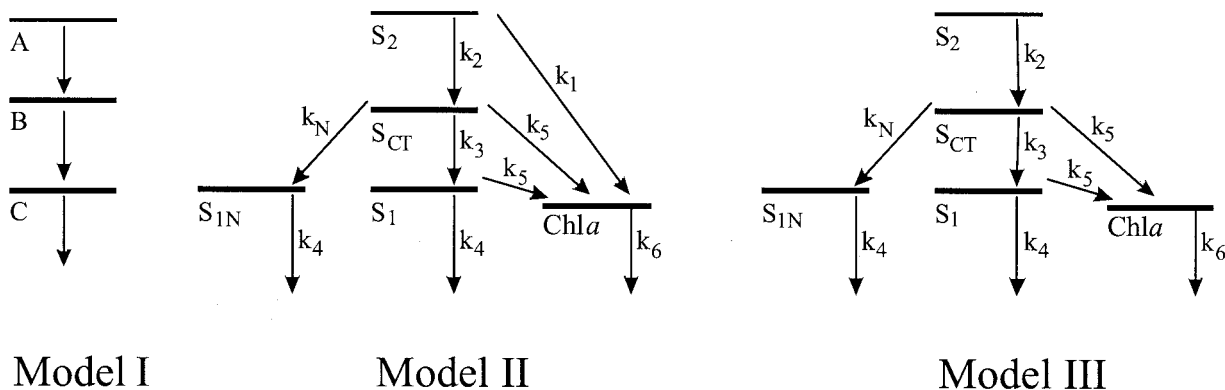


FIGURE 3 The three models used in data analysis. The three excited states of model I correspond to mixtures of the actual excited species present in PCP. The excited states of models II and III correspond more closely with pure PCP species, as do the rates connecting them. The S_{1N} state represents a population of peridinin that does not transfer energy to Chla, whereas the S_2 , S_{CT} , and S_1 states represent peridinin that do transfer energy to Chla. Note that the S_{CT} state may represent either an individual excited state or simply vibrationally excited S_1 population. Models II and III are identical aside from k_1 .

a time scale of 5 ps, concomitant with a small red shift of the Chla bleach (Kleima et al., 2000b). These observations were corroborated by measurements at 77 K (S. S. Lampoura, unpublished).

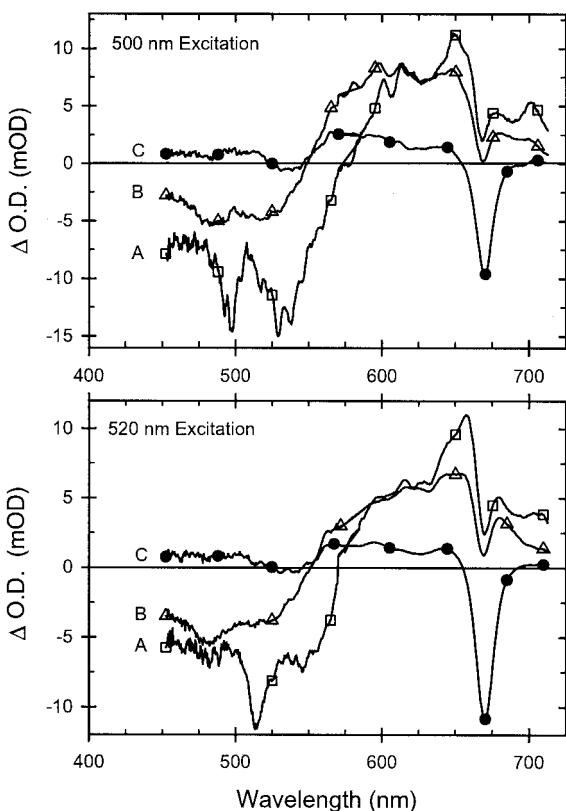


FIGURE 4 Species-associated difference spectra (SADS) estimated from fitting model I to the isotropic excitation data. \square , species A; \triangle , species B; \bullet , species C. The average characteristic lifetimes from all data sets are <200 fs for $A \rightarrow B$, 2.0 ± 0.2 for $B \rightarrow C$, and >1 ns for the decay of C.

DISCUSSION

The results mentioned briefly above will be discussed here in terms of the flow of energy within peridinin, between peridinin, and between peridinin and Chla. Thus, this section will discuss peridinin internal conversion (k_2 , k_3 , and k_4), peridinin-peridinin EET (anisotropy decay), peridinin S_2 -Chla EET (k_1), peridinin S_1/S_{CT} -Chla EET (k_4 and k_5), followed by the identity of the peridinin S_1/S_{CT} -Chla donor state.

Peridinin internal conversion

The description of internal conversion in carotenoids has been made significantly more complex recently by the observation of the $1B_u^-$ state in several bacterial carotenoids (Sashima et al., 1999, 2000) and the similar observation of the S_{CT} state in peridinin (Bautista et al., 1999a; Frank et al., 2000). In accordance with these works, our models II and III both represent peridinin internal conversion as a sequential process, from S_2 to S_{CT} to S_1 . However, because of the complexity of our model and the poor resolution of our data at early times, we cannot confidently identify S_{CT} as a separate excited state, and it may simply correspond to a vibrationally excited S_1 population. We only know that the dynamics captured by the data requires two states in the models.

The Bautista et al. (1999a) study of peridinin in various solutions does provide compelling evidence for the existence of the S_{CT} state by showing two bands of ESA with quite different solvent dependence. The $S_n \leftarrow S_1$ band (550–600 nm) is only slightly dependent on solvent, whereas the $S_n \leftarrow S_{CT}$ band (600–700 nm) is highly dependent on solvent. Bautista et al. (1999a) found that the S_{CT} state was populated rapidly (<50 fs) from S_2 and that S_{CT} and S_1 decayed together with a single lifetime. Because the S_{CT}

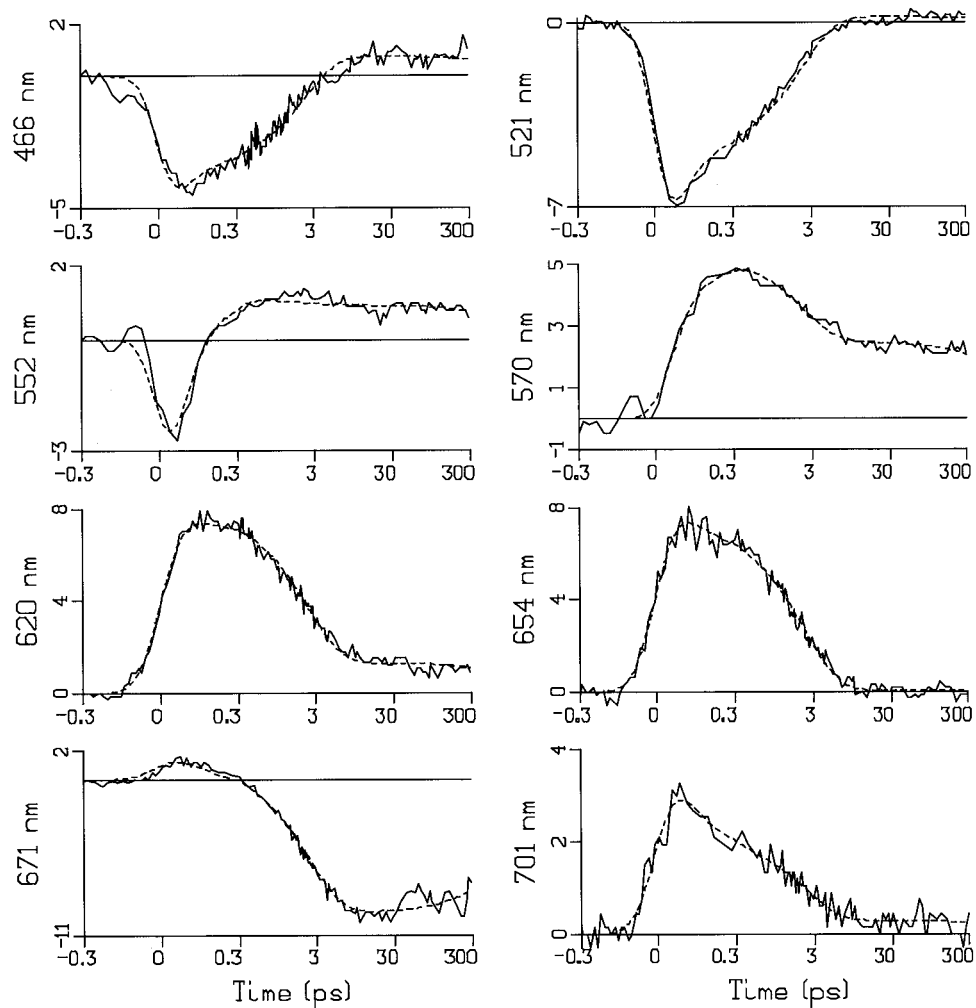


FIGURE 5 Magic angle (isotropic) data (—) and model (---) traces for several probe wavelengths from the 500-nm excitation data. Model traces derive from the model I SADS given in Fig. 4. The 521-nm traces primarily represent peridinin S_2 bleach; 570-nm traces represent peridinin $S_n \leftarrow S_1$ excited-state absorption; and 671-nm traces represent Chl a Q_y bleach. Note that the time axis is linear from -0.3 to 0.3 ps and logarithmic from 0.3 to 300 ps.

and S_1 states show the same dynamics (other than at very early times where our data cannot resolve them), we should not expect to be able to identify them separately in our models, and both the S_{CT} and S_1 states should appear spectrally similar. This is consistent with the Bautista et al. (1999a) results, and in fact, we note the strong similarity between the shape of our S_{CT} and S_1 SADS in models II and III (apart from the Chl a bleach) and the SADS reported for polar solvents in Fig. 7 of the Bautista et al. (1999a) work. This spectral similarity suggests that the protein environment in PCP is similar to low-molecular-weight alcohols. In these solvents, peridinin displays S_1 lifetimes of 12–50 ps, in accord with the ~ 15 -ps found here for k_4 . Thus, we feel that our data are most consistent with the S_2 - S_{CT} - S_1 picture of Bautista et al. (1999a) and couch our discussion in these terms.

Peridinin-peridinin interactions

The anisotropy measurements presented here afford an excellent opportunity to observe energy transfer between peridinins. We find that the anisotropy drops from 0.40 to 0.29 ± 0.05 as the population goes from peridinin S_2 to S_1/S_{CT} , suggesting that either some peridinin S_2 - S_2 EET has occurred or that the S_1/S_{CT} transition moment is oriented quite differently from the S_2 transition moment. Previous work with other carotenoids has shown deviation in the directions of the $S_n \leftarrow S_1$ and $S_2 \leftarrow S_0$ transition dipoles. For instance, Andersson and co-workers used anisotropy measurements to determine that the S_1 and S_2 transition dipoles are 23° apart in both okenone and M15, a β -carotene derivative (Andersson and Gillbro, 1995; Andersson et al., 1996). If we assume peridinin also shows this kind of

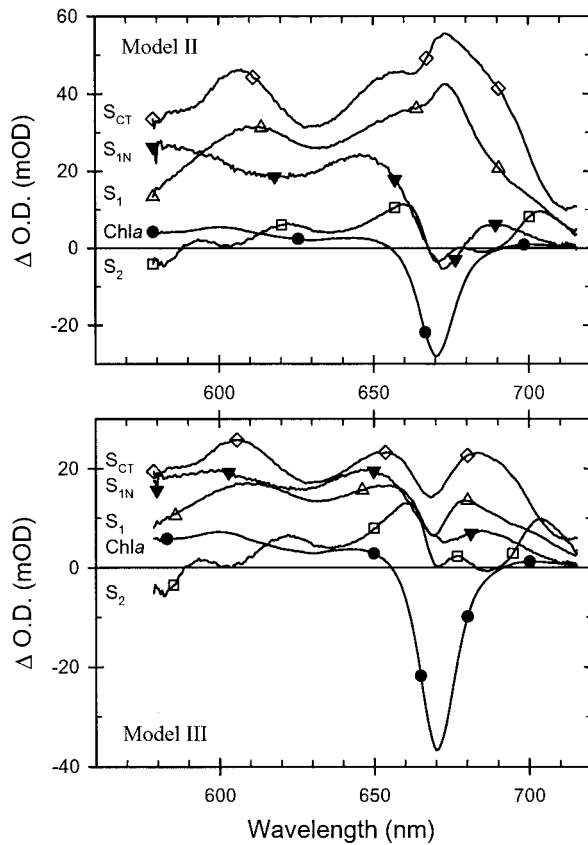


FIGURE 6 SADS from fitting the 500-nm excitation data to model II (top) and model III (bottom). Blue portions of the SADS are not shown, revealing more detail in the Chla region. In both plots, SADS traces correspond to species as follows: \square , S_2 ; \diamond , S_{CT} ; \triangle , S_1 ; \blacktriangledown , S_{1N} ; \bullet , Chla. Inverse rate constants estimated from the fits are given in Table 1.

deviation, then the 0.40–0.29 depolarization represents an angle of 25° between the S_2 and S_1 transition dipoles, in remarkable agreement with the carotenoids studied by Andersson et al. However, calculations by Damjanović et al. (2000) suggest rapid peridinin S_2 -peridinin S_2 EET, ~ 100 fs, which could compete effectively with the < 200 -fs peridinin S_2 lifetime. Either deviation between S_2 and S_1 transition dipoles or peridinin S_2 - S_2 EET is itself a plausible explanation for the observed 0.40 to 0.29 depolarization, and neither can be excluded by our data.

Once the population has left the peridinin S_2 state, fits with time-dependent S_1/S_{CT} anisotropy yield no improvement over fits with constant anisotropy. In fact, because the wavelengths shown in Fig. 7 each reflect a very different contribution from Chla relative to peridinin, as a group they are a very sensitive test of the accuracy of the anisotropy model. For instance, the 630-nm traces have little Chla signal and should reflect peridinin S_1/S_{CT} - S_1/S_{CT} EET in their anisotropy decay whereas the 670-nm traces should reflect peridinin S_1/S_{CT} -Chla EET. The success of the constant-anisotropy fit at all wavelengths (in addition to those

shown in Fig. 7) suggests that peridinin S_1/S_{CT} population is transferred directly to Chla and that peridinin S_1/S_{CT} - S_1/S_{CT} EET is a minor or negligible pathway. Though the absolute time scales are a bit different than presented here and the S_{CT} state was not considered, semi-empirical calculations (Damjanović et al., 2000) found that peridinin S_1 - S_1 EET is roughly an order of magnitude slower than peridinin S_1 -Chla Q_y EET, in qualitative agreement with our findings. Although we cannot rule out peridinin S_1/S_{CT} - S_1/S_{CT} EET, our models do not require it, and calculations suggest that it should be a minor or negligible process.

Peridinin S_2 -Chla EET

Based on other light-harvesting antenna, peridinin S_2 -Chla EET might be expected to be a significant process, but this

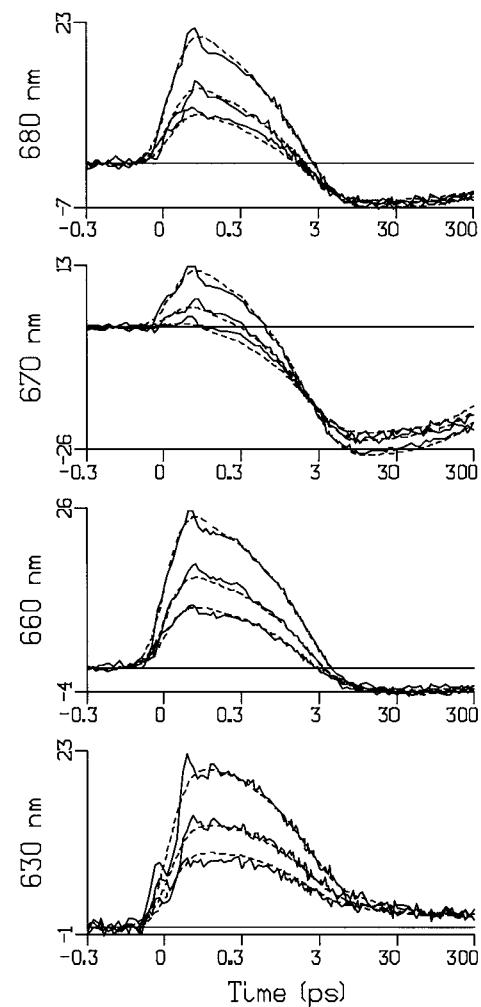


FIGURE 7 Anisotropy data (—) and model (---) traces from the 500-nm excitation data. The 630-, 660-, 670-, and 680-nm probe wavelengths demonstrate the quality of the model II fit for all polarizations. For all plots, the parallel traces have the largest absolute magnitude, magic angle intermediate, and perpendicular the least. Note that the time axis is linear from -0.3 to 0.3 ps and logarithmic from 0.3 to 300 ps.

TABLE 1 Inverse values of the rate constants connecting states in model II

Pathway	k_1	k_2	k_3	k_4^*	k_5	k_6
Model II	0.1 (<0.2)	0.1 (<0.2)	0.1 (<0.2)	15 (10–30)	2.3 ± 0.2	>1000

These times are taken from the fitting of all data sets. Values for model III are within the uncertainty ranges of the model II time scales except for the k_1 pathway, which is ∞ by definition. As noted in the text, k_N does not represent a physical EET pathway, and its value is not given. All values are times in picoseconds.

* k_4 was fixed at a value determined by fitting the red region only.

has not been observed in previous work on PCP. The overlapping features of the Chla bleach and the S_1/S_{CT} ESA make resolving early time dynamics at 670 nm difficult, as demonstrated by the 660–680-nm traces in Figs. 5 and 7 that show a total positive signal at early times giving way to a negative signal at long times. Without other data, the individual contributions of positive and negative signals cannot be separated from their sum. Because of the full spectral information in our data, we can now see that Chla bleach is present at early times and have designed models II and III to test whether this signal results from peridinin S_2 -Chla EET or from an instantaneous process. Model II allows the EET to occur, whereas model III does not, instead allowing a small (5%) initial population of excited Chla. (Note that we do not state whether the acceptor state in peridinin S_2 -Chla EET is Q_x or Q_y . Our data only identify Chla ground state bleaching, so Q_x and Q_y populations are indistinguishable and we model them together as simply excited Chla.)

The initially excited Chla population in model III may represent direct excitation by the pump pulse (perhaps into the red tail of the Soret absorption) or some other instantaneous mechanism such as an electrochromic shift. Either of these direct excitation mechanisms is plausible, although they should both be very small in magnitude. Similar experiments utilizing similar excitation wavelengths (Gradinaru et al., 2000) do not show measurable instantaneous Chla bleaching in LHC-II or CP29. Although electrochromic shifts have been observed in carotenoid bands following bacteriochlorophyll excitation in LH2 (Gradinaru et al., 1998; Herek et al., 1998), recent Stark measurements in our laboratory indicate that the magnitude of the Chla band shift signal is <0.5 mOD (R. N. Frese, unpublished results), an order of magnitude or more smaller than the initial Chla bleach seen here. Therefore, we expect instantaneous Chla bleaching to be small, but cannot rule it out completely and use an initial excited Chla population of 5% in model III.

Comparison of the SADS in Fig. 6 shows small but significant differences in the models II and III peridinin SADS near 670 nm. The model III SADS all show clear bleaching at 670 nm, suggesting that excited Chla is present in the data that is not accounted for in the model. In fact, an initial Chla population of $\sim 35\%$ is needed to remove the Chla signal from the peridinin SADS in model III. In contrast, the S_2 , S_{CT} , and S_1 SADS for Model II are free of Chla bleach. Thus, direct excitation of Chla without S_2 -Chla EET is unable to account for the 670-nm bleach present in the data at early times. Only by including S_2 -Chla EET (or an unrealistically high instantaneous Chla excitation) can the appearance of Chla signal be removed from the peridinin SADS.

In addition, the two models differ significantly in their final Chla populations. The distributions of initial excitation throughout all of the states in models II and III are given in Table 2. The overall peridinin to Chla EET efficiency in model II is 86%, very similar to the $88 \pm 2\%$ from steady-state measurements (Bautista et al., 1999b). In contrast, the corresponding efficiency in model III is 72% (including the 5% initial Chla population). Modifying the rates in model III can give a higher peridinin-Chla EET efficiency, but this requires significantly reducing k_N , resulting in a reduced S_{IN} population that, to maintain a reasonable fit to the data, drives the S_{IN} SADS to unrealistically large amplitudes. Only by including peridinin S_2 -Chla EET can good agreement between the overall peridinin-Chla EET efficiency of the model and the measured value be achieved while maintaining realistic SADS for all species.

In summary, both models II and III fit the data well, with SADS that generally appear as expected. However, the presence of Chla bleach in the peridinin SADS of model III, despite allowing instantaneous excitation of Chla, indicates the need for peridinin S_2 -Chla EET. The model II peridinin SADS appear free of Chla character, and the overall peri-

TABLE 2 Fractions of initial excitation that reach each of the states in models II and III

State	Peridinin							Chla				
	S_2	S_{CT}	S_{IN}	S_1	S_0 (S_{IN})	S_0 (S_1)	S_0 (total)	From S_2	From S_{CT}	From S_1	Initial	Total
Model II	1.00	0.50	0.10	0.38	0.10	0.04	0.14	0.50	0.02	0.34	0	0.86
Model III	0.95	0.95	0.18	0.73	0.18	0.10	0.28	0	0.04	0.63	0.05	0.72

dinin-Chla EET efficiency is reproduced significantly better by model II than model III.

The peridinin S_2 -Chla EET time scale (k_1) on the order of 100 fs is poorly determined by the combination of our data and a complex model but is similar to time scales found for the same pathway in the LH2 complexes of bacterial systems (Shreve et al., 1991; Andersson et al., 1996; Ricci et al., 1996; Krueger et al., 1998) and in LHC-II of green plants (Peterman et al., 1997a). Given the similarity of carotenoid and chlorophyll transition moment magnitudes and molecular separations in PCP compared with all of these light-harvesting complexes, it seems reasonable that the peridinin S_2 -Chla EET time scale should be similar as well. Although recent calculations on PCP found a significantly slower time scale of ~ 10 ps (Damjanović et al., 2000), they were hampered by difficulties estimating spectral overlaps and Chla transition moments. Therefore, we suggest that peridinin S_2 -Chla EET is a significant pathway in PCP with a time scale on the order of 100 fs and accounting for roughly 25–50% of the overall peridinin to Chla energy transfer.

Peridinin S_1/S_{CT} -Chla energy transfer

The remainder of the peridinin-Chla EET must be mediated by peridinin S_1/S_{CT} -Chla EET. The lifetimes associated with the SADS allow us to estimate the time scale and mechanism for peridinin S_1/S_{CT} -Chla EET, one of the primary motivations of this work. The presence of two low-lying excited singlet states, S_1 and S_{CT} , casts doubt on which is the energy donor state. For the moment we use S_D to refer to the generic peridinin donor state, leaving its identity for the next section. We emphasize that the methods used below to determine the properties of S_D are equally appropriate whether it is S_1 or S_{CT} and that because the two states decay together (Bautista et al., 1999a), the target analysis does not differentiate between them (i.e., S_1 in models II and III actually represents a mixture of S_1 and the long-lived S_{CT}). Our primary assumption is that the donor state is the same state observed in emission, a reasonable one given that the peridinin emission is measurable and that coupling involving a transition dipole easily dominates other coupling mechanisms. Along these lines, Bautista et al. (1999a) measured the fluorescence quantum yield and lifetime of peridinin in several solutions. The resulting radiative rates range from 5.4×10^6 to 2.1×10^7 s $^{-1}$. Because there is significant uncertainty about the states involved and the frequencies of the transitions, Bautista et al. (1999a) did not use these rates to estimate a transition dipole magnitude. However, for our purposes we desire an order-of-magnitude estimate and use the simple-minded assumption that the emission maxima correspond to the transition frequencies. This yields an S_D transition dipole on the order of 2 D, sufficiently large to reassure us that dipole-

dipole Coulombic coupling should dominate the total coupling (see below).

The results of fitting to models II and III give us directly an estimate of the S_D to Chla EET time scale as 2.3 ± 0.2 ps, giving a rate of $k_5 = (4.4 \pm 0.4) \times 10^{11}$ s $^{-1}$. In addition, the S_1 lifetime in the absence of energy transfer is approximately given by the decay of the non-energy-transferring peridinin population, S_{1N} as 15 ps, ranging from 10 to 30 ps, for a rate of $k_4 = 6.8 (3.2, 10) \times 10^{10}$ s $^{-1}$. This S_{1N} lifetime must be used with care because this population of peridinin may not be completely disconnected and may demonstrate slow EET to Chla. In addition, because the S_{1N} SADS is significantly contaminated with Chla features, the measured S_{1N} lifetime may also be tainted by Chla dynamics. However, although the measured value for k_4 corresponds only loosely with the peridinin S_1 - S_0 internal conversion rate, we expect effects from EET and Chla dynamics to be negligible compared with the large uncertainty given for k_4 . As mentioned previously, the shape of the S_1 and S_{CT} SADS suggest a solvent environment consistent with the measured k_4 , and, the overall peridinin-Chla EET efficiency, of which k_4 is a key component, reproduces previous measurements (Bautista et al., 1999b). Thus, we have confidence that our estimate of k_4 is reasonable.

Using the relationship of S_D lifetime to solvent polarity (Bautista et al., 1999a) suggests that a lifetime, $(k_4)^{-1}$, of 10–30 ps results from a local protein environment with a dielectric constant in the mid-twenties. Within the list of solvents described by Bautista et al. (1999a), this is similar to acetone ($\epsilon = 20.7$, $n = 1.36$), ethanol ($\epsilon = 24.3$, $n = 1.36$), and benzonitrile ($\epsilon = 25.3$, $n = 1.53$), which seem reasonable for describing the pigment environment in PCP as, in addition to protein, both lipids and water appear near the pigments in the crystal structure (Hofmann et al., 1996). In addition, these solvents, particularly benzonitrile, which should have polarizability similar to protein, suggests an index of refraction value of ~ 1.5 , which agrees well with the 1.6 ± 0.1 estimated by careful analysis of the Chla-Chla EET in PCP (Kleima et al., 2000a).

With reasonable confidence in the rates pertinent to S_D - Q_y EET, particularly the 2.3 ± 0.2 ps EET time scale, we can now estimate the strength of the coupling between the transitions. In the weak coupling limit, the rate of EET is given by (Förster, 1965):

$$k_{DA} = \frac{1}{\hbar^2 c} |V_{DA}|^2 J_{DA} \quad (2)$$

where \hbar is Planck's constant (divided by 2π), c is the speed of light, V_{DA} is the electronic coupling between the donor and acceptor transitions, and J_{DA} is their spectral overlap. The spectral overlap is given by the integral over energy of the donor emission and acceptor absorption spectra (Förster, 1965):

$$J_{\text{DA}} = AB \int \frac{f_{\text{D}}(\nu)}{\nu^3} \frac{\epsilon_{\text{A}}(\nu)}{\nu} d\nu, \quad (3)$$

where A and B are normalization constants chosen to satisfy $A \int (f_{\text{D}}(\nu)/\nu^3) d\nu = B \int (\epsilon_{\text{A}}(\nu)/\nu) d\nu = 1$. To estimate the spectral overlap, we have utilized the solution (methanol) emission spectrum of peridinin and absorption spectrum of Chla (see Fig. 2).

Normally, care must be taken to ensure that both the absorption and emission spectra reflect the homogeneous line widths of the two species. However, when the spectra show significant vibronic structure, the width of each vibronic band becomes much less important than the number and relative amplitudes of the vibronic bands. The peridinin vibronic structure, barely detectable in the emission spectrum because each band is extremely broad, is well described by a single Gaussian component. Thus, we represent the peridinin S_{D} emission by one Gaussian, centered at $14,170 \text{ cm}^{-1}$ with a width of 2800 cm^{-1} , corresponding to the width of the Franck-Condon envelope. In contrast, the well studied Chla absorption profile is quite complex. However, because the peridinin emission is much broader than the Chla absorption, the spectral overlap is insensitive to its precise description; we represent Chla as four Gaussian components for the main and first three vibronic bands. Note that the spectral overlap is driven by the main band, but the vibronic components are needed for proper normalization of that band. The Chla absorption was fit to four Gaussians centered at $14,915$, $16,000$, $17,085$, and $18,450 \text{ cm}^{-1}$, with widths of 250 , 500 , 500 , and 750 cm^{-1} and relative amplitudes of 1.000 , 0.017 , 0.087 , and 0.040 . The 250-cm^{-1} width of the Chla main band is the homogeneous linewidth of Chla in LHC-II as measured by fluorescence line narrowing (Peterman et al., 1997b) and photon echo (Agarwal et al., 2000) experiments. The relative widths of the other bands roughly match the relative widths observed in the absorption spectrum, although the final spectral overlap is insensitive to the widths of the Chla bands; widths two times larger yield a spectral overlap that is $<1\%$ different. The calculated spectral overlap is $1.65 \times 10^{-4} \text{ cm}$, which along with an inverse rate of $2.3 \pm 0.2 \text{ ps}$ yields (from Eq 2) a coupling strength of $47 \pm 2 \text{ cm}^{-1}$.

These values represent the magnitude of the total coupling between the peridinin S_{D} and Chla Q_{y} transitions, but do not give us any direct information concerning the mechanism(s) of the coupling. As mentioned at the beginning of this section, the transition dipole-transition dipole Coulombic coupling of Förster (1965) should be dominant. However, the short-range orbital overlap component has been suggested to be significant in other carotenoid systems (Scholes et al., 1997; Krueger et al., 1998, 1999a) and could be driven in PCP by the van der Waals contacts between peridinin and Chla shown in the crystal structure (Hofmann et al., 1996).

The role of orbital overlap coupling between carotenoids and chlorophylls has been recently addressed (Nagae et al., 1993; Scholes et al., 1997; Damjanović et al., 1999). All three works examined purple bacterial LHCs and determined that exchange coupling (Dexter, 1953) is negligible. In addition, a similar analysis on PCP (Damjanović et al., 2000) recently found that exchange coupling is also negligible in this system. However, a number of groups have pointed out that the exchange coupling term is the least significant of several coupling mechanisms that depend on orbital overlap (Koutecky and Paldus, 1963; Choi et al., 1964; Azumi and McGlynn, 1965; Harcourt et al., 1994; Scholes et al., 1995). Of principle importance to carotenoids are the polarization coupling and charge transfer coupling mechanisms. Using the Scholes et al. (1997) formalism along with the average peridinin-Chla separation of $\sim 10 \text{ \AA}$, we estimate that the total orbital overlap coupling for the average peridinin-Chla pair is roughly 15 cm^{-1} . Although this is a difficult contribution to estimate, previous work on LH2 using this same approach yielded EET rates that were in reasonable agreement with experiment (Krueger et al., 1998; Scholes and Fleming, 2000). Assigning $15 \pm 5 \text{ cm}^{-1}$ of the total $47 \pm 2 \text{ cm}^{-1}$ coupling to orbital overlap contributions leaves $32 \pm 7 \text{ cm}^{-1}$ that must be contributed by Coulombic coupling.

In principle, this Coulombic coupling contains all terms of the multipole expansion (e.g., dipole-dipole, dipole-quadrupole, quadrupole-quadrupole). However, because we expect the S_{D} transition dipole moment to have a significant magnitude, the dipole-dipole term should adequately represent the total Coulombic coupling,

$$V^{\text{Coul}} \approx V^{\text{dip-dip}} = \frac{\kappa}{4\pi\epsilon_0} \frac{|\mu_{\text{D}}||\mu_{\text{A}}|}{n^2R^3}, \quad (4)$$

and allow us to roughly estimate the magnitude of the peridinin donor state transition dipole, μ_{D} . Taking the peridinin S_{D} transition dipole to point along the conjugated portion of the molecule (from C9 to C20, with the center defined as the average of C7, C9, C11, and C23 from the crystal structure) suggests orientation factor κ values of -1.42 , 1.02 , 0.56 , and -0.07 for the four peridinin-Chla Q_{y} pairs. The peridinin with the smallest κ will not significantly participate in the dipole-dipole coupling, so we estimate a single, effective κ of 1.0 by averaging the absolute magnitudes of the three largest values. Finally, taking μ_{A} to be 5.2 D (Kleima et al., 2000b), R to be 10.2 \AA , and n to be 1.5 gives a peridinin S_{D} transition dipole moment of $\sim 3 \text{ D}$.

The orientation factors above, as well as calculations by Damjanović et al. (2000), suggest that the S_{D} -Chla EET is roughly separable into two time scales, possibly explaining our need for both the S_1 and $S_{1\text{N}}$ states. Thus, the S_1 and $S_{1\text{N}}$ states of models II and III may primarily correspond to the three peridinins with efficient S_{D} -Chla EET and the fourth peridinin with poor S_{D} -Chla EET, respectively. This fourth

peridinin does have reasonably good S_2 - Q_x orientation, $\kappa = -0.54$, so this peridinin with low S_D -Chla EET efficiency may well have high S_2 -Chla EET efficiency (Damjanović et al., 2000).

Identity of the peridinin donor state

Although the above analysis is fraught with the use of many approximations, it does provide a reasonable experimental measure of the properties of the peridinin donor state and is consistent with the radiative rates measured by Bautista et al. (1999a). However, as noted above, there is no clear indication as to which state is the donor.

Two recent works suggest that the S_1 state may be the energy donor. Semi-empirical calculations on peridinin (Damjanović et al., 2000) estimate an S_1 transition dipole of 4.7 D. This remarkably large transition dipole suggests that the ~ 3 D estimated here is reasonable for the S_1 transition. In addition, experimental work on the bacterial light-harvesting carotenoids lycopene, spheroidene, and neurosporene (Zhang et al., 2000) reveals measurable S_1 transition dipoles of 0.64, 0.72, and 0.86 D, respectively. This trend of increasing dipole strength with decreasing conjugation length (11, 10, and 9 double bonds) suggests that a fairly symmetric carotenoid of peridinin's size should have an S_1 transition dipole on the order of 1 D. Given the significant asymmetry of peridinin, ~ 3 D seems, again, reasonable. However, if the S_1 transition dipole is really ~ 3 D, then it should be easily visible in the PCP absorption spectrum; yet, thorough spectroscopic analyses (Carbonera et al., 1999; Frank et al., 2000; Kleima et al., 2000b) failed to find evidence of the S_1 transition in absorption or circular dichroism.

Distortion of the peridinin structure on excitation, common for polyenes (Zechmeister, 1962), would be expected to yield an emitting/donating S_1 transition with significantly more dipole strength than the absorbing transition. Such distortion could also explain a significant transition strength for S_{CT} , as has been suggested (Bautista et al., 1999a), as well as the absence of such a state from the semi-empirical calculations (Damjanović et al., 2000). Hence, distortion or twisting of the peridinin after excitation may drive the donor state transition strength, in either S_1 or S_{CT} .

Clearly, more work is needed to sufficiently explain the photophysics of peridinin. Although significant evidence suggests that the S_1 state is responsible for the EET to Chla, too many questions remain for a definitive assignment.

CONCLUSIONS

The results presented here suggest that there is significant (25–50%) energy transfer directly from the peridinin S_2 state to Chla, as well as through a low-lying singlet state, S_1 or S_{CT} , after internal conversion from the peridinin S_2 state.

Although our data cannot discriminate between direct $S_2 \rightarrow S_1$ internal conversion and the $S_2 \rightarrow S_{CT} \leftrightarrow S_1$ pathway, the latter is more consistent with the body of literature on peridinin. A small amount of depolarization, from 0.40 to 0.29 ± 0.05 , occurs on the same time scale as the S_2 - S_{CT}/S_1 internal conversion. This depolarization suggests that the $S_n \leftarrow S_{CT}/S_1$ transition dipole is oriented $\sim 25^\circ$ away from the $S_2 \leftarrow S_0$ transition dipole or that a small amount of peridinin S_2 -peridinin S_2 energy transfer occurs.

Assuming the $S_2 \rightarrow S_{CT} \leftrightarrow S_1$ pathway, the peridinin population is in equilibrium between two low-lying singlet states, S_1 and S_{CT} , after internal conversion. There is no clear evidence as to which of these is the state observed in emission, or which is the donor state in energy transfer to Chla, although some data suggest S_1 is the more likely candidate.

Fitting with the peridinin S_1/S_{CT} anisotropy fixed at 0.29 and allowing it to be time dependent gives the same results, a strong indication that significant peridinin S_1/S_{CT} -peridinin S_1/S_{CT} energy transfer does not occur before peridinin S_1/S_{CT} -Chla energy transfer. Target analysis of the isotropic decays reveals that the peridinin S_1/S_{CT} lifetime in the absence of EET is 15 (10–30) ps and that the peridinin S_1/S_{CT} to Chla EET time scale is 2.3 ± 0.2 ps. The full set of rates determined by the target analysis yields an overall peridinin-Chla EET efficiency of 86%, in agreement with that measured by steady-state methods as $88 \pm 2\%$ (Bautista et al., 1999b). In turn, this suggests a total peridinin S_1/S_{CT} -Chla coupling of $47 \pm 2 \text{ cm}^{-1}$. Assuming that $15 \pm 5 \text{ cm}^{-1}$ of this total coupling is mediated by orbital overlap mechanisms and that the remainder is driven by a dipole-dipole mechanism results in an estimate for the peridinin S_1/S_{CT} transition dipole magnitude of ~ 3 D. In addition, the 15-ps S_1/S_{CT} lifetime in PCP (in the absence of EET) suggests that the pigment environment is described by an index of refraction of ~ 1.5 in reasonable agreement with the 1.6 ± 0.1 found by studying Chla-Chla EET (Kleima et al., 2000a).

The highly efficient peridinin-Chla energy transfer process in PCP is mediated through both the peridinin S_2 transition and the lower donor transition, either S_1 or S_{CT} . Both EET pathways are mediated mainly by Coulombic coupling with the accepting Chla transition. The Coulombic coupling of the S_1 or S_{CT} transition is driven by the asymmetry of peridinin, and perhaps distortion in the excited state, allowing the donor state a significant transition moment. Lack of peridinin-peridinin EET suggests that each peridinin is independently coupled to the central Chla, quite unlike the highly cooperative situation found in purple bacterial LH1 and LH2.

We thank Frank Sharples for assisting in sample preparation, F. Kleima and H. van Amerongen for enlightening discussions, as well as A. Damjanović for additional discussions and for providing a preprint of Damjanović et al. (2000).

This work was funded by the Netherlands Organization for Scientific Research (NWO) via the Board of Earth and Life Sciences (ALW). B.P.K. was supported by a visitor fellowship from the research institute for Condensed Matter Physics and Spectroscopy (COMPAS). R.G.H. was supported by the Australian Research grant A00000264.

REFERENCES

- Agarwal, R., B. P. Krueger, G. D. Scholes, M. Yang, J. Yom, L. Mets, and G. R. Fleming. 2000. Ultrafast energy transfer in LHC-II revealed by three-pulse photon echo peak shift measurements. *J. Phys. Chem. B.* 104:2908–2918.
- Akimoto, S., S. Takaichi, T. Ogata, Y. Nishimura, I. Yamazaki, and M. Mimuro. 1996. Excitation energy transfer in carotenoid-chlorophyll protein complexes probed by femtosecond fluorescence decays. *Chem. Phys. Lett.* 260:147–152.
- Andersson, P. O., S. M. Bachilo, R.-L. Chen, and T. Gillbro. 209. 1995. Solvent and temperature effects on dual fluorescence in a series of Carotenoids: energy gap dependence of the internal conversion Rate. *J. Phys. Chem.* 99:16199–16116.
- Andersson, P. O., R. J. Cogdell, and T. Gillbro. 1996. Femtosecond dynamics of carotenoid-to-bacteriochlorophyll *a* energy transfer in the light-harvesting antenna complexes from the purple bacterium *Chromatium purpuratum*. *Chem. Phys.* 210:195–217.
- Andersson, P. O., and T. Gillbro. 1995. Photophysics and dynamics of the lowest excited singlet state in long substituted polyenes with implications to the very long-chain limit. *J. Chem. Phys.* 103:2509–2519.
- Andersson, P. O., T. Gillbro, L. Ferguson, and R. J. Cogdell. 1991. Absorption spectral shifts of carotenoids related to medium polarizability. *Photochem. Photobiol.* 54:353–360.
- Azumi, T., and S. P. McGlynn. 1965. Energy of excimer luminescence. III. Group theoretical considerations of molecular exciton and charge resonance states. *J. Chem. Phys.* 42:1675–1680.
- Bautista, J. A., R. E. Connors, B. B. Raju, R. G. Hiller, F. P. Sharples, D. Gosztola, M. R. Wasielewski, and H. A. Frank. 1999a. Excited state properties of peridinin: observation of a solvent dependence of the lowest excited singlet state lifetime and spectral behavior unique among carotenoids. *J. Phys. Chem. B.* 103:8751–8758.
- Bautista, J. A., R. G. Hiller, F. P. Sharples, D. Gosztola, M. R. Wasielewski, and H. A. Frank. 1999b. Singlet and triplet energy transfer in the peridinin-chlorophyll-*a*-protein from *Amphidinium carterae*. *J. Phys. Chem. A.* 103:2267–2273.
- Brand, L., J. R. Knutson, L. Davenport, J. M. Beechem, R. E. Dale, D. G. Walbridge, and A. A. Kowalczyk. 1985. Time-resolved fluorescence spectroscopy: some applications of associative behavior to studies of proteins and membranes. In *Spectroscopy and the Dynamics of Molecular Biological Systems*. P. Bayley, and R. E. Dale, editors. Academic Press, London. 259–305.
- Britton, G., and A. Young. 1993. Carotenoids in Photosynthesis. Chapman and Hall, London, New York. 498.
- Carbonera, D., G. Giacometti, U. Segre, E. Hofmann, and R. G. Hiller. 1999. Structure-based calculations of the optical spectra of the light-harvesting peridinin - chlorophyll *a* - protein complexes from *amphidinium carterae* and *heterocapsa pumaea*. *J. Phys. Chem. B.* 103: 6349–6356.
- Choi, S.-I., J. Jortner, S. A. Rice, and R. Silbey. 1964. Charge-transfer exciton states in aromatic molecular crystals. *J. Chem. Phys.* 41: 3294–3306.
- Chynwat, V., and H. A. Frank. 1995. The application of the energy gap law to the S_1 energies and dynamics of carotenoids. *Chem. Phys.* 194: 237–244.
- Clayton, R. K. 1980. Photosynthesis: physical mechanisms and chemical patterns. Cambridge University Press, New York.
- Damjanović A., T. Ritz, and K. Schulten. 1999. Energy transfer between carotenoids and bacteriochlorophylls in light-harvesting complex II of purple bacteria. *Phys. Rev. E.* 59:3293–3311.
- Damjanović A., T. Ritz, and K. Schulten. 2000. Excitation energy transfer in the peridinin-chlorophyll-protein of *Amphidinium carterae*. *Biophys. J.* 79:1695–1705.
- DeCoster, B., R. L. Christensen, R. Gebhard, J. Lugtenburg, R. Farhoosh, and H. A. Frank. 1992. Low-lying electronic states of carotenoids. *Biochim. Biophys. Acta.* 1102:107–114.
- Dexter, D. L. 1953. A theory of sensitized luminescence in solids. *J. Chem. Phys.* 21:834–850.
- Förster, T. 1948. Intermolecular energy transference and fluorescence. *Ann. Phys.* 2:55–75.
- Förster, T. 1965. Delocalized excitation and excitation transfer. In *Modern Quantum Chemistry*. O. Sinanoglu, editor. Academic Press, New York. 93–137.
- Frank, H. A., J. A. Bautista, J. Josue, Z. Pendon, R. G. Hiller, F. P. Sharples, D. Gosztola, and M. R. Wasielewski. 2000. Effect of the solvent environment on the spectroscopic properties and dynamics of the lowest excited states of carotenoids. *J. Phys. Chem. B.* 104:4569–4577.
- Frank, H. A., and R. J. Cogdell. 1996. Carotenoids in photosynthesis. *Photochem. Photobiol.* 63:257–264.
- Frank, H. A., R. Farhoosh, M. L. Aldema, B. Decoster, R. L. Christensen, R. Gebhard, and J. Lugtenburg. 1993. Carotenoid-to-bacteriochlorophyll singlet energy transfer in carotenoid-incorporated B850 light-harvesting complexes of *Rhodobacter sphaeroides* R-26.1. *Photochem. Photobiol.* 57:49–55.
- Fujii, R., K. Onaka, M. Kuki, Y. Koyama, and Y. Watanabe. 1998. The $2A(g^-)$ energies of all-trans-neurosporene and spheroidene as determined by fluorescence spectroscopy. *Chem. Phys. Lett.* 288:847–853.
- Govindjee. 2000. Milestones in photosynthesis research. In *Probing Photosynthesis: Mechanism, Regulation and Adaptation*. M. Younis, U. Pathre, and P. Mohanty, editors. Taylor and Francis, London. 9–39.
- Gradinaru, C. C., I. H. M. van Stokkum, A. A. Pascal, R. van Grondelle, and H. van Amerongen. 2000. Identifying the pathways of energy transfer between carotenoids and chlorophylls in LHCII and CP29: a multicolor, femtosecond pump-probe study. *J. Phys. Chem. B.* 104: 9330–9342.
- Gradinaru, C. C., I. H. M. van Stokkum, R. van Grondelle, and H. van Amerongen. 1998. Ultrafast absorption changes of the LHCII carotenoids upon selective excitation of the chlorophylls. In *Photosynthesis: Mechanisms and Effects*. G. Garab, editor. Kluwer Academic Publishers, Dordrecht, The Netherlands. 277–280.
- Harcourt, R. D., G. D. Scholes, and K. P. Ghiggino. 1994. Rate expressions for excitation transfer. II. Electronic considerations of direct and through-configuration exciton resonance interactions. *J. Chem. Phys.* 101:10521–10525.
- Herek, J. L., T. Polivka, T. Pullerits, G. J. S. Fowler, C. N. Hunter, and V. Sundström. 1998. Ultrafast carotenoid band shifts probe structure and dynamics in photosynthetic antenna complexes. *Biochemistry.* 37: 7057–7061.
- Hofmann, E., P. M. Wrench, F. P. Sharples, R. G. Hiller, W. Welte, and K. Diederichs. 1996. Structural basis of light harvesting by carotenoids: peridinin-chlorophyll-protein from *Amphidinium carterae*. *Science.* 272: 1788–1791.
- Hudson, B. S., B. E. Kohler, and K. Schulten. 1982. Linear polyene electronic structure and potential surfaces. In *Excited States*. E. C. Lim, editor. Academic Press, New York. 1–95.
- Jonas, D., M. J. Lang, T. Joo, Y. Nagasawa, Y. Jia, J. R. Norris, and G. R. Fleming. 1996. Pump-probe polarization anisotropy study of femtosecond energy transfer within the photosynthetic reaction center of *Rhodobacter sphaeroides* R26. *J. Phys. Chem.* 100:12660–12673.
- Kleima, F. J., E. Hofmann, B. Gobets, I. H. M. van Stokkum, R. van Grondelle, K. Diederichs, and H. van Amerongen. 2000a. Forster excitation energy transfer in peridinin-chlorophyll-*a*-protein. *Biophys. J.* 78:344–353.
- Kleima, F. J., M. Wendling, E. Hofmann, E. J. G. Peterman, R. van Grondelle, and H. van Amerongen. 195. 2000b. Peridinin chlorophyll *a* protein: relating structure and steady-state spectroscopy. *Biochemistry.* 39:5184–5185.

- Koepke, J., X. Hu, C. Muenke, K. Schulten, and H. Michel. 1996. The crystal structure of the light-harvesting complex II (B800–850) from *Rhodospirillum rubrum*. *Structure*. 4:581–597.
- Koutecky, J., and J. Paldus. 1963. A study of the interaction between two ethylene molecules by semi-empirical complete configuration interaction method in the π -electron approximation. *Theor. Chim. Acta*. 1:268–281.
- Koyama, Y., M. Kuki, P. O. Andersson, and T. Gillbro. 1996. Singlet excited states and the light-harvesting function of carotenoids in bacterial photosynthesis. *Photochem. Photobiol.* 63:243–256.
- Krueger, B. P., G. D. Scholes, I. R. Gould, and G. R. Fleming. 1999a. Carotenoid mediated B800–B850 coupling in LH2. *Phys. Chem. Commun.* 8:(<http://www.rsc.org/ej/qu/1999/C9903172/index.htm>)
- Krueger, B. P., G. D. Scholes, R. Jimenez, and G. R. Fleming. 1998. Electronic excitation transfer from carotenoid to bacteriochlorophyll in the purple bacterium *Rhodospseudomonas acidophila*. *J. Phys. Chem. B*. 102:2284–2292.
- Krueger, B. P., J. Yom, P. J. Walla, and G. R. Fleming. 1999b. Observation of the s_1 state of spheroidene in LH2 by two-photon fluorescence excitation. *Chem. Phys. Lett.* 310:57–64.
- Kühlbrandt, W., D. N. Wang, and Y. Fujiyoshi. 1994. Atomic model of plant light-harvesting complex by electron crystallography. *Nature*. 367: 614–621.
- McDermott, G., S. M. Prince, A. A. Freer, A. M. Hawthornthwaite-Lawless, M. Z. Papiz, R. J. Cogdell, and N. W. Isaacs. 1995. Crystal structure of an integral membrane light-harvesting complex from photosynthetic bacteria. *Nature*. 374:517–521.
- Mimuro, M., U. Nagashima, S. Takaichi, Y. Nishimura, I. Yamazaki, and T. Katoh. 1992. Molecular structure and optical properties of carotenoids for the in vivo energy transfer function in the algal photosynthetic pigment system. *Biochim. Biophys. Acta*. 1098:271–274.
- Nagae, H., T. Kakitani, T. Katoh, and M. Mimuro. 1993. Calculation of the excitation transfer matrix elements between the S_2 or S_1 state of carotenoid and the S_2 or S_1 state of bacteriochlorophyll. *J. Chem. Phys.* 98:8012–8023.
- Peterman, E. J. G., R. Monshouwer, I. H. M. van Stokkum, R. van Grondelle, and H. van Amerongen. 1997a. Ultrafast singlet excitation transfer from carotenoids to chlorophylls via different pathways in light-harvesting complex II of higher plants. *Chem. Phys. Lett.* 264: 279–284.
- Peterman, E. J. G., T. Pullerits, R. van Grondelle, and H. van Amerongen. 1997b. Electron-phonon coupling and vibronic fine structure of light-harvesting complex II of green plants: temperature dependent absorption and high-resolution fluorescence spectroscopy. *J. Phys. Chem. B*. 101:4448–4457.
- Polivka, T., J. L. Herek, D. Zigmantas, H.-E. Akerlund, and V. Sundström. 1999. Direct observation of the (forbidden) S_1 state of carotenoids. *Proc. Natl. Acad. Sci. U.S.A.* 96:4914–4917.
- Ricci, M., S. E. Bradforth, R. Jimenez, and G. R. Fleming. 1996. Internal conversion and energy transfer dynamics of spheroidene in solution and in the LH-1 and LH-2 light-harvesting complexes. *Chem. Phys. Lett.* 259:381–390.
- Sashima, T., Y. Koyama, T. Yamada, and H. Hashimoto. 2000. The $1B_u^+$, $1B_u^-$, and $2A_g^-$ energies of crystalline lycopene, beta-carotene, and mini-9-beta-carotene as determined by resonance-Raman excitation profiles: dependence of the $1B_u^-$ state energy on the conjugation length. *J. Phys. Chem. B*. 104:5011–5019.
- Sashima, T., H. Nagae, M. Kuki, and Y. Koyama. 1999. A new singlet-excited state of all-trans-spheroidene as detected by resonance-Raman excitation profiles. *Chem. Phys. Lett.* 299:187–194.
- Sashima, T., M. Shiba, H. Hashimoto, H. Nagae, and Y. Koyama. 1998. The $2A_g^-$ energy of crystalline all-trans-spheroidene as determined by resonance-Raman excitation profiles. *Chem. Phys. Lett.* 290:36–42.
- Scholes, G. D., and G. R. Fleming. 2000. On the mechanism of light harvesting in photosynthetic purple bacteria: B800 to B850 energy transfer. *J. Phys. Chem. B*. 104:1854–1868.
- Scholes, G. D., R. D. Harcourt, and G. R. Fleming. 1997. Electronic interactions in photosynthetic light-harvesting complexes: the role of carotenoids. *J. Phys. Chem. B*. 101:7302–7312.
- Scholes, G. D., R. D. Harcourt, and K. P. Ghiggino. 1995. Rate expressions for excitation transfer. III. An ab initio study of electronic factors in excitation transfer and exciton resonance interactions. *J. Chem. Phys.* 102:9574–9581.
- Schubert, W.-D., O. Klukas, N. Krauss, W. Saenger, P. Fromme, and H. T. Witt. 1997. Photosystem I of *Synechococcus elongatus* at 4 Å resolution: comprehensive structure analysis. *J. Mol. Biol.* 272:741–769.
- Sharples, F. P., P. M. Wrench, K. Ou, and R. G. Hiller. 1996. Two distinct forms of the peridinin-chlorophyll a-protein from *Amphidinium carterae*. *Biochim. Biophys. Acta*. 1276:117–123.
- Shreve, A. P., J. K. Trautman, H. A. Frank, T. G. Owens, and A. C. Albrecht. 1991. Femtosecond energy-transfer processes in the B800–B850 light-harvesting complex of *Rhodobacter sphaeroides* 2.4.1. *Biochim. Biophys. Acta*. 1058:280–288.
- Sundström, V., T. Pullerits, and R. van Grondelle. 1999. Photosynthetic light-harvesting: reconciling dynamics and structure of purple bacterial LH2 reveals function of photosynthetic unit. *J. Phys. Chem. B*. 103: 2327–2346.
- van Grondelle, R., J. P. Dekker, T. Gillbro, and V. Sundström. 1994. Energy transfer and trapping in photosynthesis. *Biochim. Biophys. Acta*. 1187:1–65.
- van Stokkum, I. H. M., T. Scherer, A. M. Brouwer, and J. W. Verhoeven. 1994. Conformational dynamics of flexibility and semirigidly bridged electron donor-acceptor systems as revealed by spectrotemporal parameterization of fluorescence. *J. Phys. Chem.* 98:852–866.
- Zechmeister, L. 1962. *Cis-Trans Isomeric Carotenoids Vitamins A and Arylpolyenes*. Springer-Verlag, Vienna.
- Zhang, J.-P., R. Fujii, P. Qian, T. Inaba, T. Mizoguchi, Y. Koyama, K. Onaka, Y. Watanabe, and H. Nagae. 2000. Mechanism of the carotenoid-to-bacteriochlorophyll energy transfer via the S_1 state in the LH2 complexes from purple bacteria. *J. Phys. Chem. B*. 104:3683–3691.